

FEDSM-ICNMM2010-1000 \*

## LUMPED PARAMETER MODELING FOR MICROFLUIDIC NETWORKS FOR REALIZING RECONFIGURABLE NANO-OPTICS ARCHITECTURES

**Seok-Won Kang**  
Texas A&M University  
College Station, TX, USA

**Hector J. De Los Santos**  
NanoMEMS Research, LLC  
Irvine, CA, USA

**Debjyoti Banerjee**  
Texas A&M University  
College Station, TX, USA

### ABSTRACT

The geometry of a microchannel (or nanochannel) has a significant effect on pressure drop due to viscous friction. In this study, we investigate the flow behavior in microfluidic network architectures where the flow occurs from a straight square main channel to tributary channels. The flow phenomena are studied for various geometries such as circular, hexagonal, rectangular, rhombohedra, square, and triangular cross-sections. We calculate the filling time of microchannels by tracking the meniscus position in capillary driven flows. For this calculation, we implement a lumped parameter model based on electrical analogies between flow resistance and viscous friction factor. The simulation of this model is conducted using MATLAB GUI (Graphic User Interface) and it enables an end-user to perform parametric studies such as the effect of hydraulic diameter, length, geometry, number of tributary channels, and properties of the working fluid. The results of simulation are verified via Computational Fluid Dynamics (CFD) simulations (VOF method). The motivation of this study is to develop relevant design tools for predicting the flow behavior in different reconfigurable microfluidic/nanofluidic network architectures for the realization of programmable photonic band gap crystals (PBC).

### INTRODUCTION

Photons have superior capability as the carriers to transmit information as a result of their highly reliable transmissibility. Photonic Crystals (PCs) are materials to control photons' flow in the same way as electrons are controlled in a semiconductor crystal [1]. Photonic Crystals, composed of periodic dielectric nanostructures, can be tuned by way of locating arrays of defects within the host periodic lattice to tailor the transmission of electromagnetic waves (EM) at specific wavelengths [2]. Band of wavelengths, within which propagation is forbidden are called photonic band gaps [2].

In general, the location of arrays of defects to program the functionality of PCs is simulated using finite-difference time-domain (FDTD) technique [1]. The formation of defects (holes filled by liquid with specific refractive index) affects the set of wavelengths and properties of band gap. Furthermore, according to the defect pattern (or the shape of designed holes to be filled), the time required to fill up the holes varies, which can cause the delay of a signal propagating through PCs. This programmable-defect array idea can be applied to the various nano-optics architectures such as optical switching, beam steering, and slow light functions. In an actual device, the dynamic reconfiguration of the location and concentration of arrays of defects can be described as the result of exploiting nanofluidic capillarity in nanochannels. The filling of the holes occurs on a row-by-row basis and Fig. 1. depicts 1-D (one dimensional) schematic of possible 1-D implantation.

In order to develop an understanding of the phenomenon filling the PC defects with a liquid, in this study we report the design of a simulation tool for investigating the flow behavior in microfluidic networks (MN). The analysis is performed using lumped parameter model based on electrical analogies between flow resistance and viscous friction factor. The liquid refractive index needs to be distinctly different from that of air for optimizing the optical performance of the PC. This simulator can be used for the future study to identify the kind of liquid with suitable refractive index, surface tension, and contact angle. The simulator is designed using MATLAB GUI (Graphic User Interface) and it enables an end-user to analyze the capillary flow in MN for a user specified geometrical architecture and material parameters (surface tension, contact angle, density, and viscosity). The simulations account for non-linear interactions such as dynamic contact angle, meniscus stretching, and meniscus bifurcation. The variation in dynamic contact angle with instantaneous flow parameters (e.g., Capillary number) is represented by an appropriate analytical model, that is discussed next.

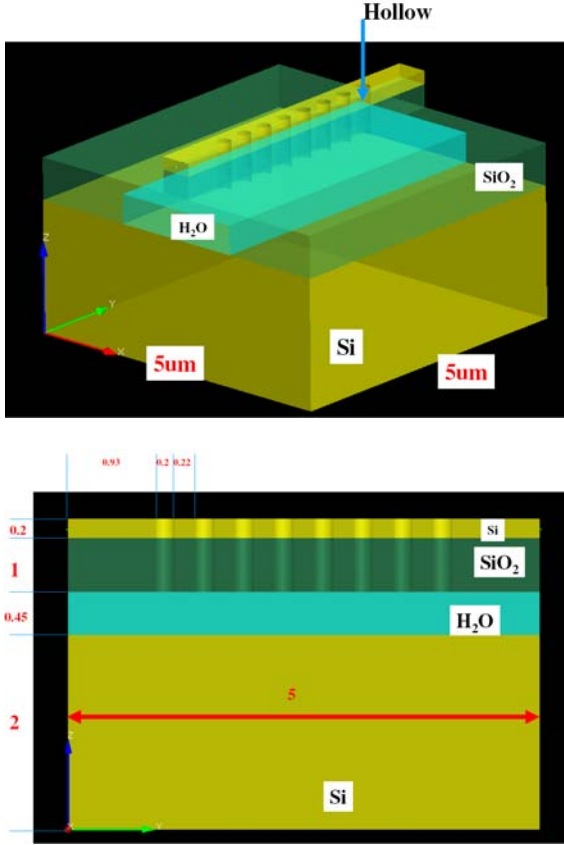


Figure 1. Schematic of possible 1-D implantation of reconfigurable PC concept

## NOMENCLATURE

$A$	Cross-sectional area, $m^2$
$C$	Darcy friction factor
$D_h$	Hydraulic diameter, $m$
$L$	Length of channel, $m$
$I_p$	Polar moment of inertia
$I_p^*$	$I_p / A^2$
$P$	Wetting perimeter, $m$
$f$	Volumetric force at the interface resulting from surface tension, $N$
$\Delta p$	Pressure drop, $N/m^2$
$t$	time, $s$
$v$	Velocity of the mixture, $m/s$
$\mu$	Dynamic viscosity, $kg/m-s$
$\nu$	Kinematic viscosity, $m^2/s$
$\rho$	Density, $kg/m^3$
$\phi$	Volumetric flow rate, $m^3/s$

## MODELING BASED ON MACRO MODEL

For a laminar flow in a straight microchannel, viscous losses dominate the pressure drop. In capillary driven flows, the pressure drop due to viscous losses is balanced by Laplace pressure from surface tension [3].

$$\Delta p = \frac{4\sigma \cos \theta}{D_h} = f_D \frac{L}{D_h} \frac{\rho u^2}{2} \quad (1)$$

Equation (2) represents the lumped parameter model based on electrical analogies, where the flow resistance is defined as the pressure drop to flow-rate ratio.

$$\Delta p = \frac{C}{2} \frac{\mu}{D_h^2} L \cdot u = \frac{C}{2} \frac{\mu}{D_h^4} L \cdot \phi = R \cdot i = e \quad (2)$$

Various types of cross section of the tributaries are explored in this study, including circular, rectangular, square, rhombus, hexagon and triangle (as listed in Fig. 2). Fig. 3 represents the equivalent network model of a microfluidic network for distributing the capillary driven flow from the main artery microchannel into the tributary microchannels.

The flow equations based on electrical analogy (Kirchhoff's Voltage Law: KVL) in the MN can be represented as the linear simultaneous equations as follows (Fig. 3):

$$R_0 u_0 + \sum_{i=1}^{n-1} R_i u_i = p_{in} + \Delta p_m \quad (3)$$

$$\sum_{i=0}^{j-1} R_i u_i + R_{Tj} u_{Tj} = p_{in} + \Delta p_T \quad \text{for } j = 1, 2, \dots, n-1 \quad (4)$$

$$A u_i - A_T u_{Tj+1} - A u_{i+1} = 0 \quad \text{for } i = 0, 1, \dots, n-2 \quad (5)$$

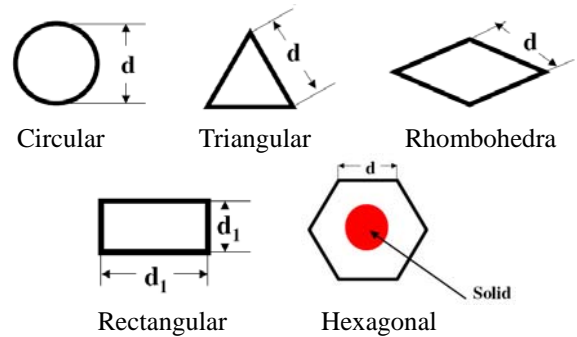


Figure 2. Microchannel cross-sections.

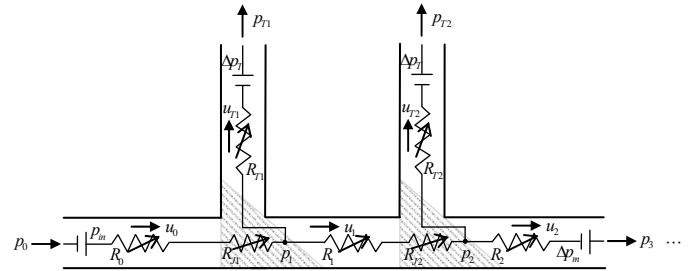


Figure 3. Macromodel corresponding to the microfluidic network (MN) shown in Fig. 1.

## FRICION FACTOR FOR CAPILLARY FLOW IN MICROCHANNELS OF ARBITRARY CROSS-SECTIONS

Various analytical models for friction factor in microchannels of arbitrary shape and aspect ratio have been proposed in the literature. The model of Shah [4] and Yilmaz [5] are similar in form, and they are based on the model developed by Bender [6] for a circular microchannel. Although these models are accurate, those are relatively difficult to adopt for our study since these models require a complex numerical solution prior to implementation [7]. Equation (6) is a compact model that provides the approximate values of the skin friction coefficient  $f_f \text{Re}_{D_h}$  (also called ‘‘Fanning friction factor’’) based on the hydraulic diameter  $D_h$  in microchannels of arbitrary cross-section [8].

$$C_f = 128\pi^2 I_p^* \frac{A}{P^2} \quad (6)$$

This model, so called as approximate polar moment of inertia model of Bahrami et al., is based on Saint-Venant principle that the friction factor calculated for the elliptical cross-section is equivalent to that of same cross-sectional area of arbitrary cross-sections. This model shows good agreements with experiment results, but it can be applied only for singly connected cross-sections [8]. The friction factor of doubly-connected geometry such as hexagonal geometry with circular core can be calculated from the equivalent rectangular model of Muzychka and Yovanovich [9] as follows:

$$C_f = 8\sqrt{\pi} \frac{(1-\beta)\sqrt{1-\beta^2}}{1+\beta^2 - \frac{(1-\beta^2)}{\ln(1/\beta)}} \frac{4\sqrt{A}}{P}, \quad \text{for } 0 < \beta < 1$$

with  $(7)$

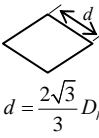
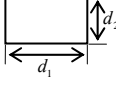
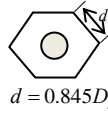
$$\beta = \sqrt{\frac{A_i}{A_o}}$$

For the fully developed, laminar, and incompressible flow, the following relationship is used to convert  $C_f \text{Re}_{D_h}$  to the Darcy friction factor  $f_D \text{Re}_{D_h}$  [10]:

$$f_D \text{Re}_{D_h} = 4C_f \text{Re}_{D_h} \quad (8)$$

Table 1 presents the predicted values of  $f_D \text{Re}_{D_h}$  for various cross-sections. For singly connected cross sections that are typically used in various experimental studies (such as in [11]) Eq. (6) is more suitable, and has been used in this study as well. Also, we adopted the model of Muzychka and Yovanovich for the doubly-connected cross-sections.

**Table 1. Values of  $f_D \text{Re}_{D_h}$  for various cross-sections**

Cross-section	$f_D \text{Re}_{D_h}$
 $d = D_h$	$A = \frac{\pi}{4}d^2$ , $P = \pi d$ , $I_p^* = \frac{1}{2\pi}$ , $f_D \text{Re}_{D_h} = 64$
 $d = \sqrt{3}D_h$	$A = \frac{\sqrt{3}}{4}d^2$ , $P = 3d$ , $I_p^* = \frac{\sqrt{3}}{9}$ , $f_D \text{Re}_{D_h} = 46.8$
 $d = \frac{2\sqrt{3}}{3}D_h$	$A = \frac{\sqrt{3}}{2}d^2$ , $P = 4d$ , $I_p^* = \frac{\sqrt{3}}{12}$ , $f_D \text{Re}_{D_h} = 39.48$
 $d_1 = \frac{3}{2}D_h = d$ , $d_2 = \frac{3}{4}D_h = \frac{1}{2}d$	$A = \frac{1}{2}d^2$ , $P = 3d$ , $I_p^* = \frac{5}{24}$ , $f_D \text{Re}_{D_h} = 58.48$
 $d = D_h$	$A = d^2$ , $P = 4d$ , $I_p^* = \frac{1}{6}$ , $f_D \text{Re}_{D_h} = 52.64$
 $d = 0.845D_h$	$A_i = \frac{\pi}{16}d^2$ , $A_o = \frac{3\sqrt{3}}{2}d^2$ , $\beta = 0.275$ , $P = 6d + \frac{1}{2}\pi d$ , $f_D \text{Re}_{D_h} = 90.01$

## NUMERICAL MODEL

The meniscus displacement with respect to time during multi-phase flows in a microchannel can be simulated numerically using the Volume-of-Fluids (VOF) method [12]. Surface tension effects in capillary flows are incorporated in the VOF method. In this method, continuity equation and momentum equation are coupled and solved simultaneously. The flow is considered to be laminar, incompressible, Newtonian and isothermal. The Navier–Stokes and continuity equations for a three dimensional flows are given as:

$$\nabla \cdot \vec{v} = 0 \quad (9)$$

$$\frac{\partial}{\partial t} \vec{v} + (\vec{v} \cdot \nabla) \vec{v} = \vec{f} - \frac{\nabla p}{\rho} + \nu \nabla^2 \vec{v} \quad (10)$$

For microchannel flows the body forces are negligible and therefore the body force terms can be eliminated to save on the

computational cost. In the VOF method, the physical properties of each fluid are calculated as weighted averages based on the volume fraction of the individual fluid in a single cell. The liquid volume fraction distribution can be determined by solving a separate passive transport equation, given as:

$$\frac{\partial F}{\partial t} + \vec{v} \cdot \nabla F = 0 \quad (11)$$

The physical properties of the mixture are derived from that of the two phases through the volume fraction function. A commercial tool (Fluent®) is used to simulate the flow behavior in the microchannel. The simulations were performed for the fluid thermo-physical properties of water, where viscosity ( $\mu$ ) is  $0.001003 \text{ kg/m-s}$ , density ( $\rho$ ) is  $998.2 \text{ kg/m}^3$ , surface tension ( $\sigma$ ) is  $0.0728 \text{ N/m}$  and contact angle ( $\theta$ ) is  $10^\circ$ . The Navier-Stokes equations in the VOF model are discretized using first-order up-winding method. The segregated solver is applied with the PISO pressure correction method. A pressure inlet boundary condition is applied with a small gauge pressure of  $20 \text{ Pa}$ . This allows for the meniscus to form and stabilize rapidly.

## RESULTS AND DISCUSSION

Numerical simulations using both VOF and linear approximation methods were conducted in order to assess the effect of channel geometry on the filling time for a single channel of various cross-sections. The length and hydraulic diameter of each micro-channel are  $3 \mu\text{m}$  and  $0.2 \mu\text{m}$ , respectively. The filling time is calculated using Eq. (1) by integrating the inverse of velocity with respect to the traveling distance [3], which shows that the filling time is increased proportionally to the value of the friction factor summarized in Table 1 for the same length and hydraulic diameter.

Papautsky et al. [12] reported an approximate 20% increase in the laminar friction constant at low microchannel aspect ratio and at low Reynolds number flows, compared to macroscale predictions from the classical Navier-Stokes theory. So, the differences in hexagonal, rhombohedra, and circular cross sections indicate that the approximate models proposed in Eq. (6) and Eq. (7) have not sufficiently reflected the micro-scale effects for the hydraulic diameter less than  $1 \mu\text{m}$ ; moreover, the polar moment of inertia model is accurate to only about 8% [6]. Nevertheless, in most cases, since the differences between macro and VOF models are within 10%. Hence, the macro model is used to simulate the capillary driven flows in conduits with cross sectional geometries listed in Fig. 4.

Fig. 6 and Fig. 7 show the plots for the meniscus position as a function of time in the artery and tributary microchannels that are obtained from the macro-model and the VOF simulations. The line plotted in pink color in Fig. 6 shows the predictions by the macro-model for a single microchannel (with no tributaries) of the same length and hydraulic diameter as the artery microchannel. The actual value of the meniscus position in the artery and tributary microchannels obtained from the

macro-model is plotted using a blue line and red lines, respectively. Moreover, The VOF simulation corresponding to each microchannel is plotted using a pair of green markers in the same plots.

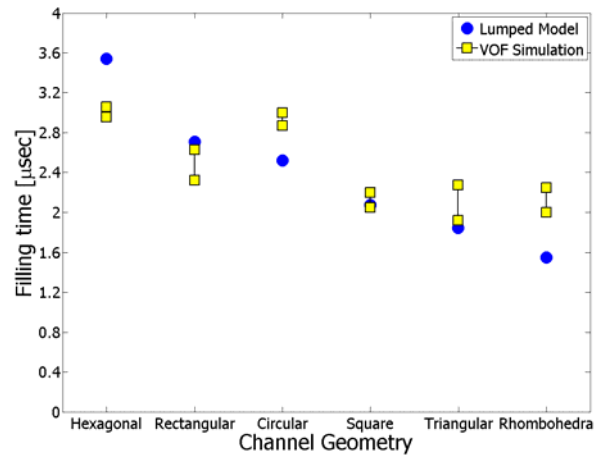


Figure 4. Filling time for single micro-channels with various cross-sections.

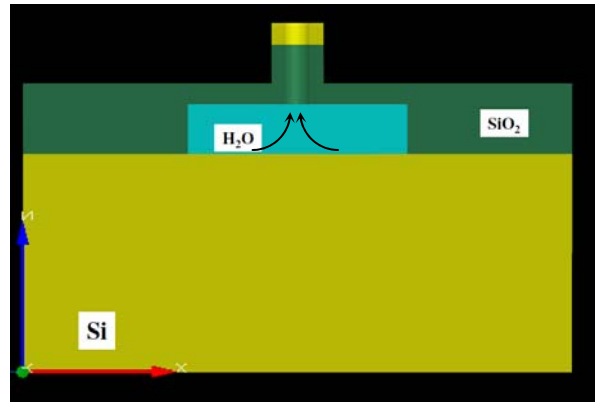
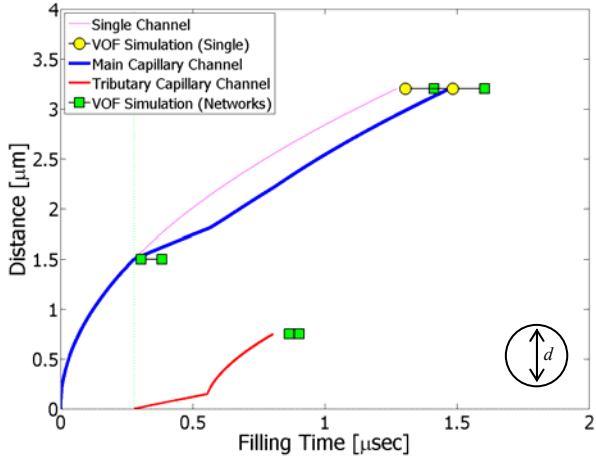
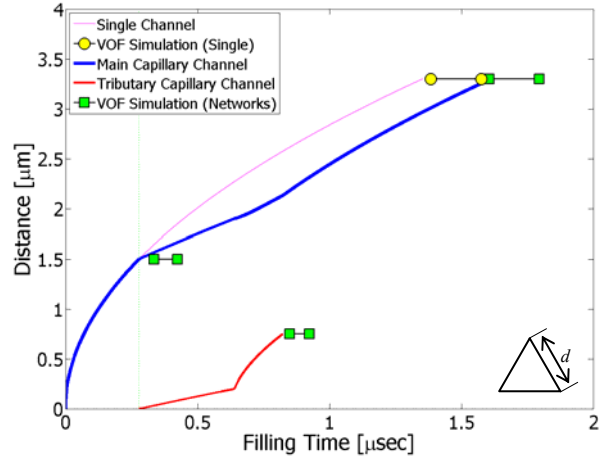


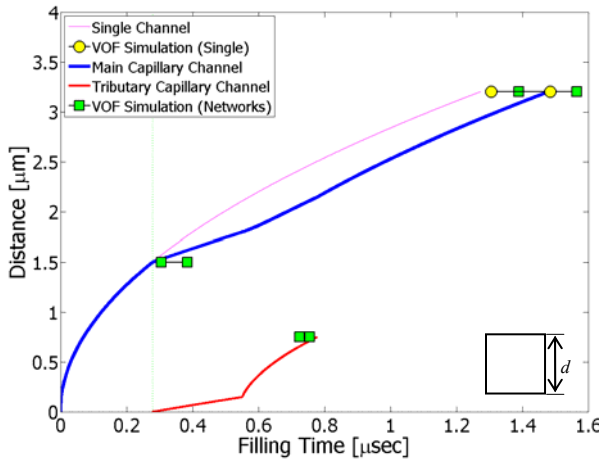
Figure 5. Simplest MN schematic expressed as T junction composed of one tributary with arbitrary cross sections.



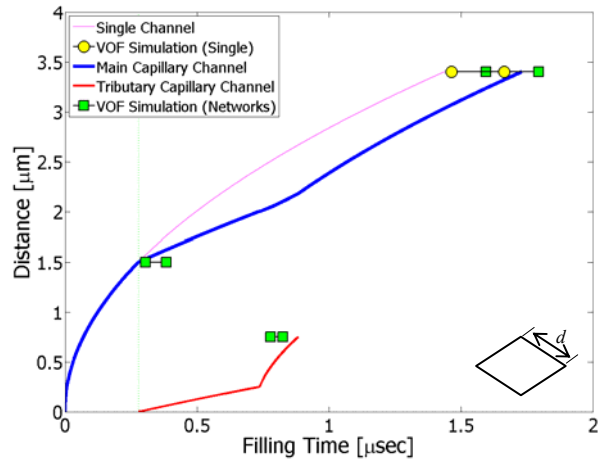
(a)



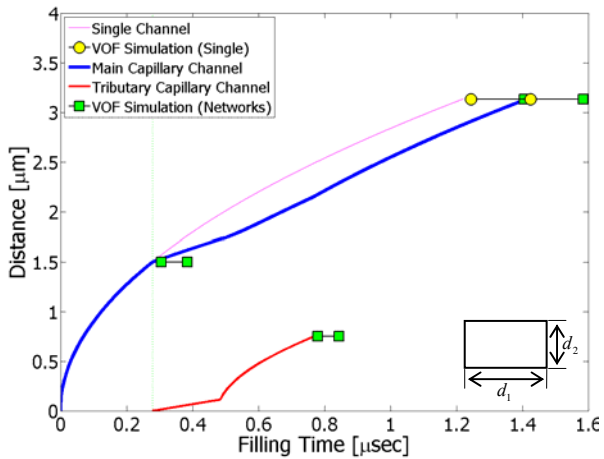
(d)



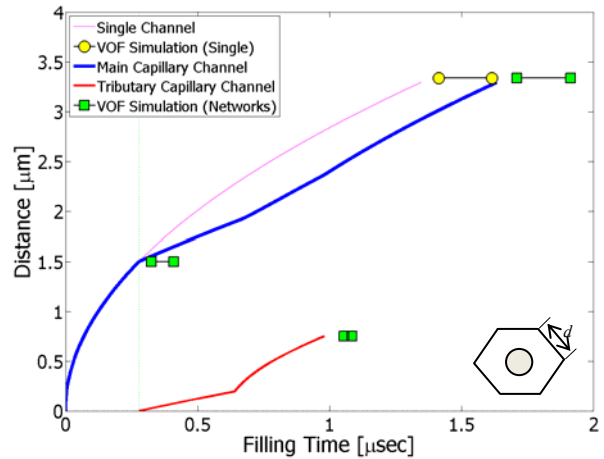
(b)



(e)



(c)



(f)

**Figure 6. Comparison of filling time between VOF simulations and Lumped-Parameter Model for the tributary with various cross-sections (a) Circular (b) Square (c) Rectangular (d) Triangular (e) Rhombohedra (f) Hexagonal.**

One of the major obstacles to the numerical validation of lumped-model is to find the appropriate behavioral representation of the meniscus in the junction between microchannels. The flow re-distribution in the junctions causes geometrical effects and variations in physical behavior such as meniscus stretching, folding and additional free surface generation which would result in additional flow resistance and impede the propagation rates of the menisci.

According to the numerical and experimental validation of A. A. Saha and S. K. Mitra [13], although the dynamic contact angle has marginal effect on the capillary flow, it significantly affects the displacement rates of menisci. To implement these effects in the lumped-model, an effective dynamic contact angle instead of static (equilibrium) contact angle can be considered only for capillary junctions. Among several theories for dynamic contact angle, the predictions from the model of Kistler [15] has been found to match the experimental data reasonably well for partially wet surfaces as well as for flows with both low and high capillary number  $Ca = \mu U / \sigma$  regime. In addition, the meniscus stretches downstream into the artery microchannel from the capillary junction area. Thus, the capillary junction area is extended until the meniscus bifurcation is completely finished. After the flow bifurcation is accomplished the meniscus in the tributary microchannel propagates towards the exit plane.

The plots in Fig. 6. show the simulation results based on the macro-model for MN with one tributary microchannel of various cross-sections as shown in Fig. 5. This simulation is to verify the feasibility of macro-model implementation into MN of various geometries. The filling time obtained from these simulations is consistent with the effects due to variation in geometry such as friction factor. The predictions from the macro-model are in good agreement with VOF simulations to within ~5 %.

From Fig. 7, in the MN simulation with 8 tributaries of circular cross-sections, it is observed the meniscus propagation rate is reduced due to meniscus formation in the junctions and a leakage in the flow from the artery to the tributary after meniscus bifurcation and subsequently recovered after finishing the filling of the tributary microchannels. The flows induced by capillary forces as the meniscus passes through the main capillary channel are shown by a blue line. As the flow bifurcates at the flow junctions and the flow is distributed into the tributary capillary channels, the capillary position in each tributary channel as a function of time is plotted using red lines. As the number of tributary channels is increased, nonlinear phenomenon affect the flow behavior - such as meniscus stretching, folding and additional free surface generation. These non-linear flow interactions affect the rate of meniscus displacements due to reduction of driving potential by viscous friction. The changes in flow behavior due to these non-linear interactions are reasonably matched by the results obtained from simulations using the macro model.

## CONCLUSIONS

In this study the efficacy of macro-models for simulating flows in MN was investigated. The macro-model formulation was derived using a simple approach based on the Kirchoff's network rules for electrical circuits. The viscous pressure drops and capillary pressures were represented by equivalent resistors and potential sources. The flow rates (or velocity values) in each leg of the network was represented by an equivalent current. The simulations were performed using MATLAB. The effect of static and dynamic contact angles were explored in this study. The effect of various channel cross sections on the flow behavior was also explored. The predictions from the macro model were validated using computational fluid dynamics (CFD) models based on the Volume of Fluids (VOF) technique. The numerical validation shows that the macro-model matched the results from the VOF model to within 5 %. Hence, this study shows that these macro-models provide a reasonable approximation for investigating flow behavior for capillary driven flows in MN with branched networks such as in MN with multiple tributaries.

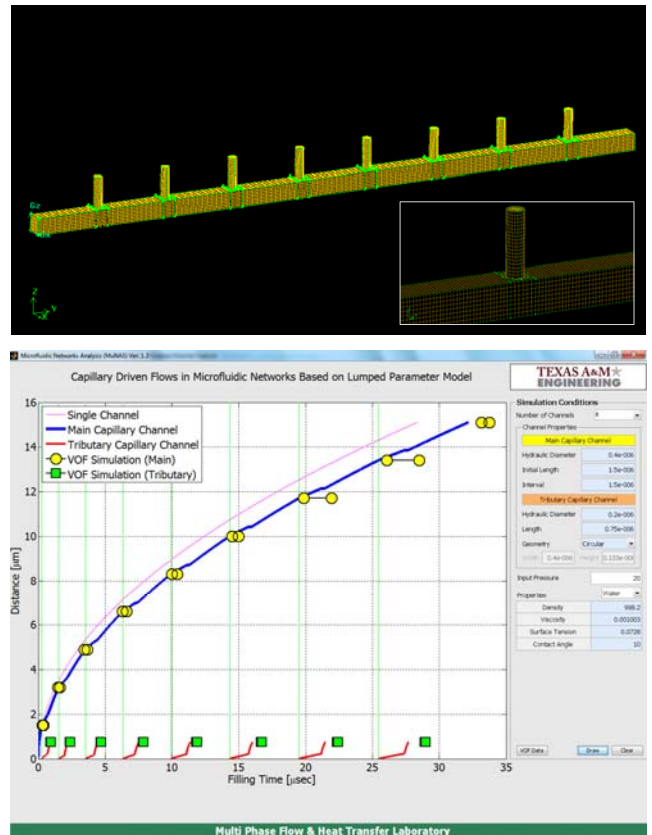


**Figure 7. (Top) MN configuration. (Bottom) Comparison of prediction for the rate of meniscus propagation from the macro-model with the results from VOF simulation, for a static contact angle of 10°.**

## ACKNOWLEDGMENTS

The authors acknowledge NanoMEMS Research LLC for supporting this study as a part of AFOSR STTR Phase I effort (Title: "Reconfigurable Materials for Photonic Systems"). The authors also acknowledge the support from DARPA Microfluidics Fundamentals Focus Center (DARPA-MF<sup>3</sup>) through the University of California at Irvine. During this study DB was partially supported by research grants from ONR, SPAWAR (US Navy), DARPA and DOE Solar Energy Program. During this study, DB (author) was also supported by a grant from the 3M Corporation as "3M Corp. Non-Tenured Faculty Fellow".

## REFERENCES

- [1] Joannopoulos, J. D., Johnson, S. G., Winn, Joshua N., and Meade, R. D., 1995, *Photonic Crystals: Molding the Flow of Light*, 2nd Edition, Princeton University Press, New Jersey.
- [2] Yablonovitch, E., 1993, "Photonic band-gap structures," *J. Opt. Soc. Am. B*, Vol. 10, No. 2, pp.283-295.
- [3] Banerjee, D., 2005, "Experimental validation of macromodels for simulating capillary driven multi-phase flows used for microchamber filling", *Proceedings of INTERPACK2005, The ASME/Pacific Rim Technical Conference and Exhibition on Integration and Packaging of MEMS, NEMS and Electronic Systems*, July 17-22, San Francisco, CA, USA.
- [4] Shah, R. K., 1975, "Laminar flow friction and forced convection heat transfer in ducts of arbitrary geometry," *Int. J. Heat Mass Transfer*, Vol. 18, pp. 849-862.
- [5] Yilmaz, T., 1990, "General Equations for Pressure Drop for Laminar Flow in Ducts of Arbitrary Cross Sections," *J. Energy Resour. Technol.*, Vol. 112, pp. 220-223.
- [6] Bender, E., 1969, "Druckverlust bei Laminarer Stromung im Rohreinlauf," *Chemie-Ingenieur Technik*, Vol. 41, pp. 682-686.
- [7] Duan, Z. and Yovanovich, M. M., 2009, "Pressure drop for laminar flow in microchannels of arbitrary cross-sections," *Semi-Therm 25 Semiconductor Thermal Measurement and Management Symposium*, pp.111-120, March 15-19, San Jose, CA, USA.
- [8] Bahami, M., Yovanovich, M. M., and Culham, J. R., 2007, "A novel solution for pressure drop in singly connected microchannels of arbitrary cross-section", *Int. J. Heat Mass Transfer*, Vol. 50, pp. 2492-2502.
- [9] Yovanovich, M. M., and Muzychka, Y. S., 1997, "Solutions of Poisson Equation within Singly and Doubly Connected Domains," *1997 National Heat Transfer Conference*, Aug. 10-12, Baltimore, MD, USA.
- [10] A.F. Mills, 1999, *Heat transfer*, 2nd Edition, Prentice Hall, Upper Saddle River, NJ.
- [11] Pfund, D., Rector, D., Shekarriz, A., Popescu, A., and Welty, J., 2000, "Pressure drop Measurements in a microchannel", *AIChE J.*, Vol. 46(8), pp. 1496-1507.
- [12] Papautsky, I., Gale, B. K., Mohanty, S., Ameen, T. A., and Frazier, A. B., 1999, "Effects of rectangular microchannel aspect ratio on laminar friction constant," *Proceedings of SPIE*, Vol. 3877, pp. 147-158.
- [13] Saha, A. A. and Mitra, S. K., 2008, *Recent advances in modeling and simulation: Chap 17 Modeling and Simulation of Microscale Flow*, 1st Edition, In Tech Education and Publishing, pp. 283-316.
- [14] Saha, A. A. and Mitra, S. K., 2009, "Effect of dynamic contact angle in a volume of fluid (VOF) model for a microfluidic capillary flow," *J. of Colloid and Interface Sci.*, Vol. 339, pp. 461-480.
- [15] Sikalo, S., Wilhelm, H. D., Roisman, I. V., Jakirlic, S. and Tropea, C., 2005, "Dynamic contact angle of spreading droplets: Experiments and simulations," *Phys. Fluids*, Vol. 17, pp. 062103-1-13.